Materials and Structures (2022) 55:179
https://doi.org/10.1617/s11527-022-01988-8

ORIGINAL ARTICLE

The immediate and short-term degradation of the wood surface in a cement environment measured by AFM

Juan Li · Bohumil Kasal

Received: 5 February 2022 / Accepted: 31 May 2022 / Published online: 10 August 2022

Abstract This study aims to measure the pit torus and border to monitor the immediate and short-term degradation of wood surfaces after the concrete is cast and the cement hydration releases heat. The surface morphology and adhesion force curves were measured by atomic force microscopy during the treatments in saturated calcium hydroxide solutions ranging from 1 h to 27 days. The results showed that the pit torus and pit border showed different degradation processes. The adhesion force was sensitive to the type of the surface chemical components exposed during the degradation, while the surface modulus, deformation and jump-off force ratio were sensitive to the surface structural strength. The surface modulus of the pit torus degraded to 0.61–0.66 of the untreated original (95% CI) after 7-h treatments, and degraded almost completely after 48-h treatments. The surface modulus of the pit border degraded to 0.83–0.95 of the untreated original (CI) after 10 days and to 0.20–0.23 of the untreated original (95% CI) after 27 days of treatments. The treatment temperature 50 °C caused a 10-times faster degradation in the torus modulus compared to the temperature 20 °C.

Keywords Pit · Calcium hydroxide solutions · AFM · Force–displacement curves

1 Introduction

Combining concrete with lignocellulosic materials such as wood and natural fibers has been considered as one of the possible methods of concrete reinforcement in civil engineering applications [1–4]. It has been shown that the alkaline environment can cause degradation of the wood chemical structural components [5, 6]. Several studies have focused on the degradation of natural fibers in a concrete matrix [2, 3, 7, 8]: the alkaline ions (Ca^{2+}, OH^-) first degraded lignin and pectin in the middle lamellae and disintegrated fibers; the peeling-off and alkaline hydrolysis reactions then degraded the cellulose micro-fibers. The degradation is a surface phenomenon and will affect the bulk properties if the alkaline environment is able to penetrate throughout the lignocellulosic material. The surface properties are critical in developing the interface between the fibers and the cementitious matrix. This work focuses on the surface properties

J. Li (✉) · B. Kasal (✉)
Division of Organic and Wood-Based Materials, TU Braunschweig, Hopfengarten 20, 38102 Braunschweig, Germany
e-mail: juan.li@tu-braunschweig.de

B. Kasal
e-mail: bohumil.kasal@wki.fraunhofer.de; kasalb@tu-bs.de

B. Kasal
Fraunhofer Wilhelm-Klauditz-Institut WKI, Bienroder Weg 54E, 38108 Brunswick, Germany

and uses wood as a model material for the lignocellulosic materials in general. We assume that the degradation of the wood surface will affect the bonding in the wood-concrete interface; Alkaline ions (Ca^{2+}, OH^{-}) are easier to transport to the depth of the wood through the degraded surface layer, thus accelerating the degradation of the material. Immediate and short-term effects of the alkaline environment on lignocellulosic materials are still not fully understood [2]. When concrete is freshly casted and the cement starts to hydrate, the released heat can cause the temperature to rise to about 40–50 °C. This temperature rise may be maintained for more than 6 days based on the volume and surrounding conditions [9]. The elevated temperature may accelerate chemical reactions between the hydration products in concrete (such as Ca^{2+}, OH^{-}) and components of the lignocellulosic material. In massive concrete elements, the accumulated heat could maintain the temperature of the material up to 70 °C for several days [10].In softwoods, there are about 50–300 pits on the radial face and in the overlap part of one tracheid cell [11]. The overarching secondary cell walls situate around the aperture in the middle, which flares into a broad pit chamber between two tracheids [12]. The pit membrane in the chamber consists of mainly celluloses with two distinct regions: a thickening non-permeable torus in the center and a circular porous margo [12, 13]. The pit border can represent the complex structure of wood secondary cell walls; the pit membrane represents the natural cellulose fibers. Therefore, we have selected bordered pits to monitor the wood surface degradations in alkaline environments.In softwoods, a main passage of the liquids occurs through the fiber cavity into a pit chamber, through the pit membrane pores, and into the next pit chamber and fiber cavity [11]. In living trees, pits account for at least 50% of the overall hydraulic resistance [14]. In the industrial use, wood drying causes irreversible pit aspirations and results in a low permeability to fluids [15]. Therefore, the degradation of pit membranes will increase the permeability of wood to the concrete pore water. Atomic force microscopy (AFM) provides nanoscale resolution in imaging and mechanical measurements of materials in natural states. This advantage of minimum sample preparation entails itself fully in biomaterial and bioresource studies, for example, without the contamination from metal coating and the distortion in vacuum in scanning electron microscopy (SEM) measurements. Some studies used AFM to characterize the ultrastructure of the pit membrane [14, 16, 17]. Only one study used functional tips to measure the changes of adhesion forces after pits were treated by heat and UV light [18]. This study used a silicon tip to measure force curves, and examined multiple parameters, such as the adhesion force, jump-off force ratio, the local surface modulus and deformation. The goals of this work were: (1) to characterize the immediate and short-term degradation of the wood surface after the concrete is freshly cast and during the curing process; (2) to establish the parameters from AFM measurements to quantitatively and qualitatively characterize the surface degradation process; (3) to characterize the accelerated effect of elevated temperature. The hypothesis was that the adhesion force was sensitive to the type of the surface chemical component exposed during the degradation process, while the local surface modulus and deformation were sensitive to the surface structural strength.

2 Methods

2.1 Materials

An air-dried Norway spruce (Picea abies) woodblock with dimensions of 8 × 5 × 50 mm (radial(R) × tangential(T) × longitudinal(L)) was cut into small samples of 3 × 3 × 5 mm (R × T × L, 20 samples in total). Six samples were randomly chosen and the radial surfaces were polished with a diamond knife (histo DH4560, Diatome Ltd, Switzerland) using a rotary microtome (HM 360, Microm, Germany). The saturated $Ca(OH)_2$ solutions (pH = 12.3) were used to simulate the alkaline environment of the cement hydration process after the concrete was freshly poured on a wood surface, and the concrete pore water during the service life. In the following analysis, the term "alkaline solution" is used to represent the saturated $Ca(OH)_2$ solutions.

2.2 Treatments

Three samples were submerged in the 300 ml alkaline solution in an air-tight glass jar at 20 °C and three at 50 °C in the oven. After each treatment, the samples were removed from the alkaline solution, rinsed by

deionized water for 10 min, and then placed in 300 ml of deionized water in a sealed glass jar for 3 days to remove the alkaline ions from the sample surface. The rinsed samples were dried with a paper tissue and then stored in a desiccator (relative humidity $< 10\%$, 21 ± 2 °C) to dry, and to stabilize for at least 48 h. Upon drying, the unremoved alkaline ions will precipitate and form $Ca(OH)_2$ crystals on the sample surface [8], which will cover the cell walls or pits, thus interfering with the AFM measurements. The rinsing strategy used in this study proved to remove the alkaline ions efficiently and the sample surfaces were free of $Ca(OH)_2$ crystals(Fig. 1). The temperature of 50 °C was chosen to study the effect of the hydration heat during cement curing, and the temperature of 20 °C was used to simulate a normal application temperature in the service life. To measure the immediate and short-term degradation processes, three samples were treated for a cumulative time of 1, 7, 48, 144, 264, and 648 h at 50 °C. Identical samples were measured and treated throughout the entire experiment. Three samples were treated at 20 °C for 1344 h to compare the accelerating effect of the temperature level.

2.3 Atomic force microscopy (AFM) measurements

The AFM Agilent Technologies 5500 (Agilent Technologies, Inc., Santa Clara, CA) device was used in this study. The measurements were conducted in an environmental chamber under the nitrogen environment with a relative humidity below 5%. The samples were in the chamber for at least 2 h to stabilize and to dry the surface before measurements. A silicon Multi75AL-G (Nanoandmore, Germany) tip was first blunted to avoid uncontrolled wear. The cantilever and the tip were imaged by scanning electron microscopy (SEM, JEOL (Germany) GmbH). The SEM images showed that the tip radius was about 50 nm (Fig. 2a, b). The force constant of the cantilever was determined to be 3 N/m using the thermal noise method, and the deflection sensitivity was 100 nm/V. The same tip was used throughout the entire experiment. The tip was continuously monitored by a silicon surface and a wood control sample and showed no change during the measurements. A typical topography image of a bordered pit in the contact mode is shown in Fig. 2c.

An area of 2.5×5 μm in the pit border and an area of 1×1 μm in the pit torus were chosen for measurements. Topography images in the contact mode and adhesion force –displacement curves of the chosen areas were developed to monitor the degradation process of the pit border and torus. On each sample 64 force curves on the pit torus and 128 curves on the pit border were measured.

2.4 Adhesion force and jump-off force ratio

The raw curve obtained from AFM measurements is the force–displacement curve, where the displacement of the piezo, i.e., the rest position of the cantilever Z is recorded [19]. There are two discontinuities in the force–displacement curve (Fig. 3), the jump-to-contact in the approach curve and the jump-off-contact in the retract curve. The jumps happen when the force gradient is larger than the force constant of the cantilever and the cantilever becomes unstable [19]. In the retract curve, the adhesion force is the maximum negative force, and we define the jump-off force ratio as the ratio between the jumping force-span and the adhesion force. We observed a regular change in the jumping force span in the retract curve, and we believe that this parameter could reflect the degradation of the

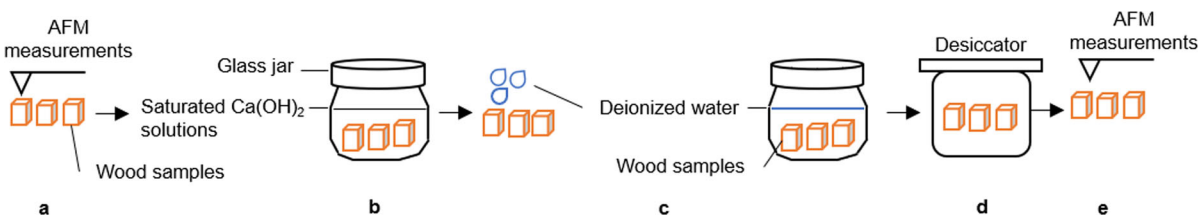

Fig. 1 Treatment process of wood samples in saturated $Ca(OH)_2$ solutions. (**a**) AFM measurements on untreated wood samples; **b** Wood samples are treated in saturated $Ca(OH)_2$ solutions in a glass jar; **c** Wood samples are washed with deionized water; **d** Wood samples are put in the desiccator (relative humidity $< 10\%$, 21 ± 2 °C); (**e**) AFM measurements on treated wood samples

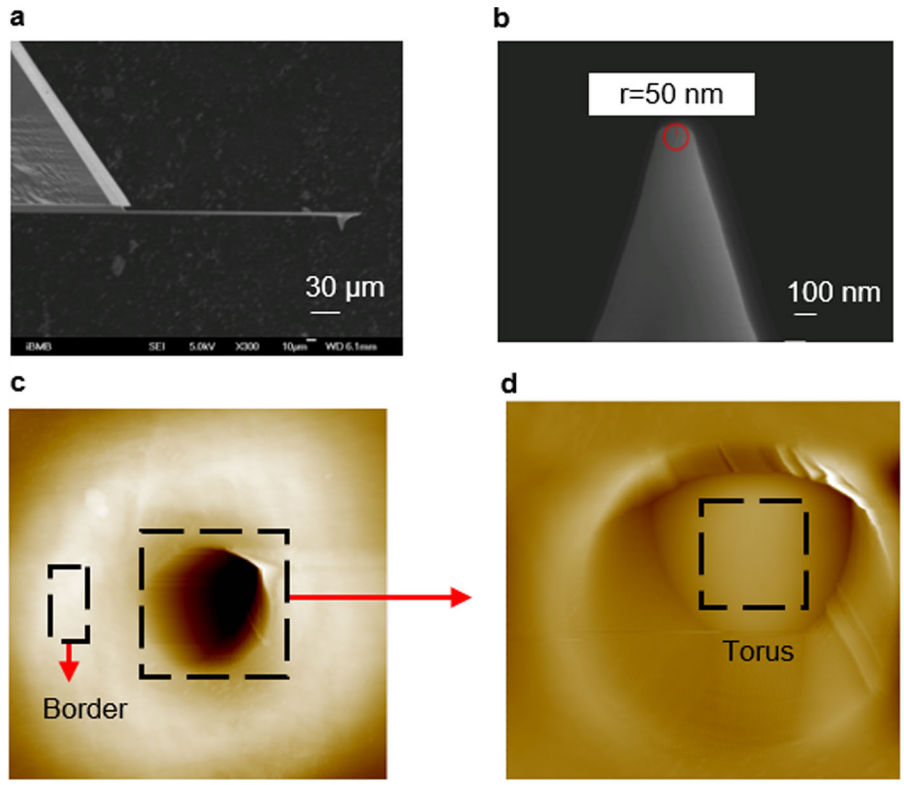

Fig. 2 The SEM image of the AFM tip and the bordered pit measured by the tip. **a** The side view of the cantilever and the tip; **b** The tip; **c** The topography image of a bordered pit (size: 20 × 20 μm); **d** The torus (size: 8 × 8 μm)

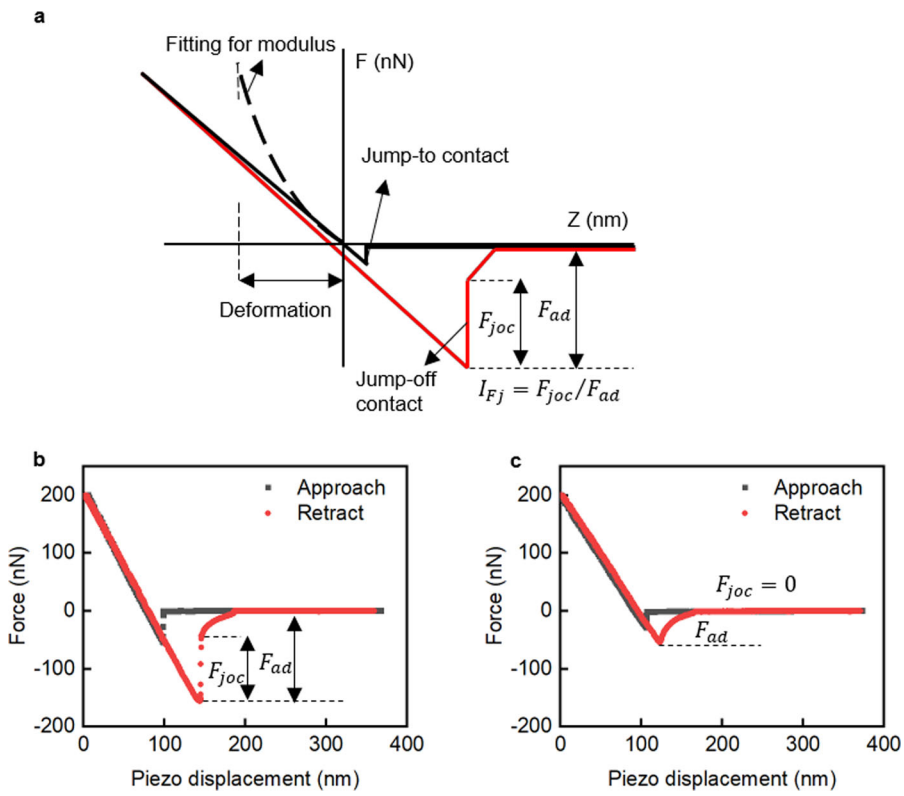

Fig. 3 The force–displacement curve. **a** The approach curve (black), the retract curve (red), and the two discontinuities: the jump-to-contact and the jump-off-contact. The jump-off force ratio (I_{Fj}) is the ratio of the jump-off force span (F_{joc}) and the adhesion force (F_{ad}): $I_{Fj} = F_{joc}/F_{ad}$; (**b**) A measured force–displacement curve from an untreated torus: the retract curve has a jump-off-contact, and the jump-off force is F_{joc}; (**c**) A measured force–displacement curve from a treated pit border: the retract curve has no jump-off-contact, and the jump-off force is 0

measured material. Given that the tip did not change during the measurements (we proved this by regularly checking the tip with a silicon surface and wood control samples), the change in the interactions between the tip and the material should be caused by the change in the material.

2.5 Local surface modulus and deformation

In the approach curve, the adhesion force (< 30 nN) was smaller than the applied load (200 nN). We therefore neglected the adhesion forces and applied Hertz model [20] to calculate the local surface modulus (Eqs. (1) and (2)). When the applied load was 3 times higher compared to the adhesion force, the difference between the modulus calculated by the Derjaguin–Muller–Toporov (DMT) and the Hertz models was less than 10%, and decreased rapidly to less than 2% with the increasing applied load [21]. It is important to note that all models are only approximations. However, the relative change of the modulus during the degradation process and not the magnitude of the modulus itself was the goal of this study. We have used the surface modulus as a measure to evaluate the change of surface properties as a result of treatments and to compare the treated and untreated samples; We did not evaluate the magnitude of this modulus as a material property in an absolute sense. We have used the following equations [20]:

$$F = \frac{4K\sqrt{R}}{3(1-\nu^2)}\delta^{3/2} \tag{1}$$

$$\frac{1}{K} = \frac{3}{4}\left(\frac{1-\nu^2}{E} + \frac{1-\nu_i^2}{E_i}\right) \tag{2}$$

where F is the applied load on the sample surface, R is the radius of the tip curvature, F is set as 200 nN and R is 50 nm (Fig. 2). δ is the sample – tip separation distance. E, E_i, ν, ν_i, are the moduli and the Poisson's ratios of the sample and the tip. E_i of the silicon tip is about 100 GPa and is much larger than the E of the wood surface (several GPa´s difference), so the latter part in Eq. (2) can be ignored. The deformation is the displacement of the tip under the applied load (200 nN) after being in contact with the surface.

2.6 Repeatable measurements

We used the identical AFM tip and measured the identical pit torus and pit border before and after each treatment. We used the relocating method that we developed in the previous paper [22], where unique pit patterns on a small sample surface were used to relocate the identical pit and the identical cell wall. Therefore, the error induced by the spatial variation across wood surfaces could be eliminated, and the changes induced by the treatments could be measured.

2.7 Data processing and statistics

The calculations of the surface modulus, deformation, adhesion force and the jump-off force ratio were performed using self-written MATLAB code. The data processing and curve fitting were conducted in Origin 2019b [23]. The statistical analysis was done by IBM SPSS Statistics [24]. The one-way ANOVA test and Duncan's multiple range test were performed at a α level of 0.05. The 5% of the lowest and highest ends of the distributions (the data of 3 samples were pooled together) was discarded, and the truncated average and variance were calculated. The confidence interval (CI) for the quotient of two means was calculated using Fieller's theorem [25] at the 95% level. The Root Mean Square (RMS) roughness of the pit border and torus surfaces were calculated by the Gwyddion software [26].

3 Results

3.1 Morphology

From the Fig. 4, it follows that the images of the torus surface show obvious degradation with treatment time at 50 °C. The untreated torus surface shows pustules in varying sizes; details show some pustules fusing together, some atop of others (Fig. 4a). Similar structures were reported with AFM tapping mode imaging [14]. With the treatment at 50 °C, the pustules become swelled, smeared and disintegrated (Fig. 4b, c, d). The RMS roughness increased from 2.6 to 3.8 nm after 264 h of treatments.

Pit border is a part of the over-arching cell wall. The untreated border surface appear amorphous. We assume that the alkaline solutions wash away the

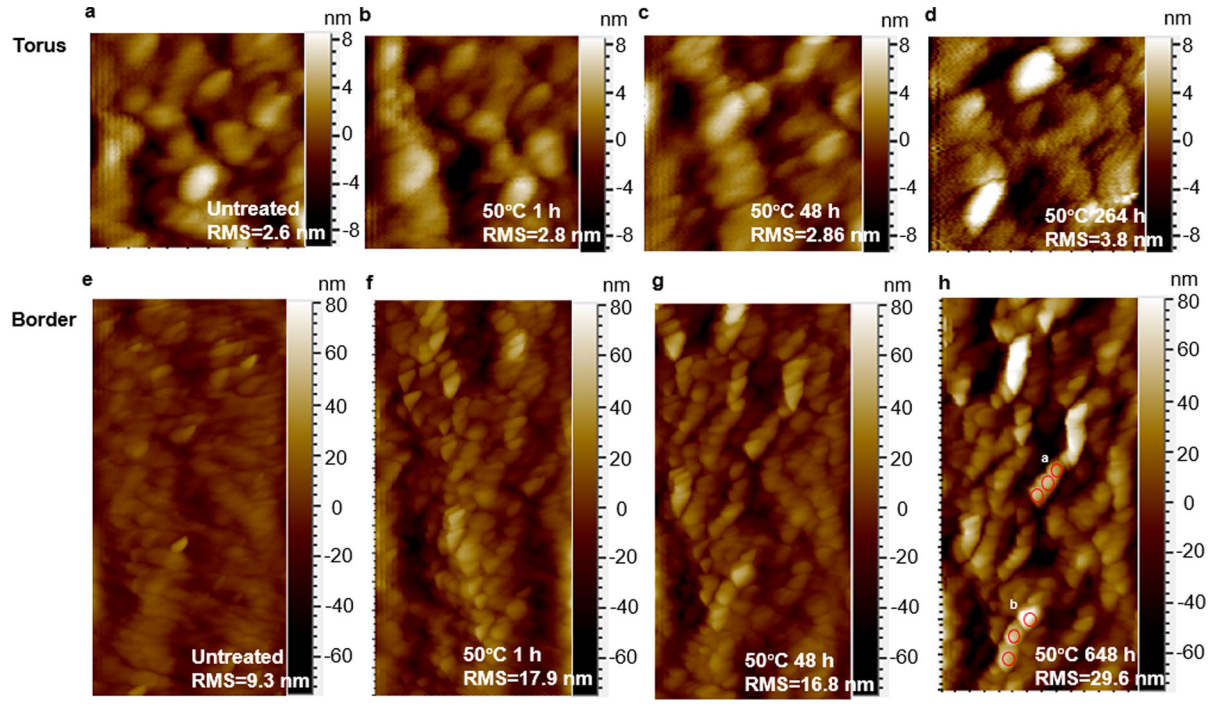

Fig. 4 The AFM topography images of the pit torus and the pit border during degradation. The pit torus image is 1 × 1 μm. The pit border image is 2.5 × 5 μm. Heights are represented by the color intensity which is shown in the vertical axes next to the figures. RMS: RMS roughness. [ab] Particles fusing into a short stick

amorphous top layer, and expose the underlying structures (Fig. 4f, g, h): particles with the size ranging from 100 to 200 nm. Some particles fuse and form a short stick as shown in Fig. 4h. The RMS roughness increased from 9.3 to 29.6 nm after 648 h of treatment (Fig. 4h). We assume that the alkaline solutions wash away the substance between the exposed particles, and result in a rougher surface. We hypothesize that the removed substance is extractives and the hemicelluloses-lignin matrix, and the particles left on the surface are clusters of cellulose aggregates. We reported the cellulose aggregates to be in the width of 40–60 nm on wood cell walls, which were exposed after the extractives and the hemicelluloses-lignin matrix were removed by heating [27]. More explanations will be given with the data on the change of adhesion forces in the latter part of the paper.

3.2 Surface modulus and deformation

The torus surfaces lost more than half of their original modulus after several hours of treatments at 50 °C; After 264 h, the modulus degraded close to 0 ($P = 0$). As shown in Fig. 5a, the one-hour treatment already caused a decrease in modulus ($P = 0.001$). Using Fieller's theorem [25], the 7-h and 48-h treatments at 50 °C degraded the surface modulus to 0.61–0.66, and 0.27–0.29 of the untreated samples (the 95% CI); the treatments at 20 °C for 1344 h degraded the surface modulus to 0.09–0.10 of the untreated samples (the 95% CI).

*: In each figure, the boxes with * are not significantly different in ANOVA tests at the 5% level (figure b, d); the boxes without * are significantly different in ANOVA tests and Dunnett's T3 tests at the 5% level.

The modulus of pit border surfaces was influenced to a much smaller degree by the treatments at 50 °C (Fig. 5b). The first 7-h treatment did not cause any significant decrease in the modulus ($P = 0.222$, untreated, 50 °C 1 h, 50 °C 7 h). The followed 257 h of treatments degraded slightly the modulus to 0.83–0.95 compared to untreated samples (the 95% CI, $P = 0.0009$). No significant differences in the modulus were found between the treatment time of 48,

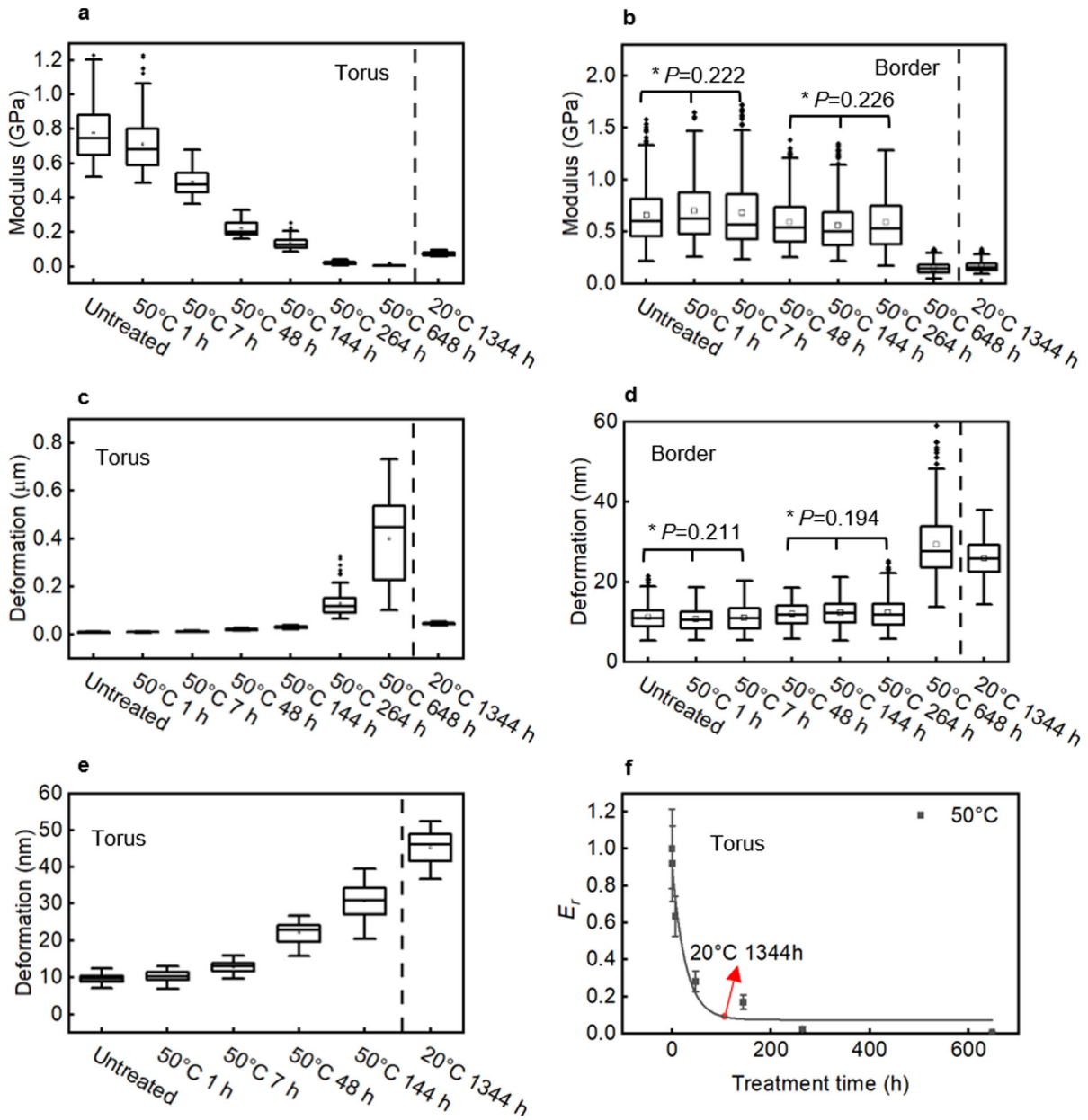

Fig. 5 The changes of the modulus and deformation of the pit torus and border with the treatment time: **a** The torus surface modulus; **b** The border surface modulus; **c** The torus surface deformation; **d** The border surface deformation; **e** The torus surface deformation without the treatment time of 264 and 648 h at 50 °C; **f** The fitted curve to the normalized residual surface modulus (E_r) of the torus at 50 °C. The vertical bars represent the standard deviation and the squares represent the average value of the residual modulus at 50 °C. The red circle represents the point on the fitted curve that corresponds to the residual modulus after treatments at 20 °C for 1344 h

144, and 264 h (P = 0.226). The extended treatment time of 648 h at 50 °C and 1344 h at 20 °C degraded the border surface modulus to less than 30% of the untreated samples (0.20–0.23 and 0.23–0.26 at the 95% CI).

The trends of deformations of the pit torus and border surfaces corresponded well with that of moduli. The untreated torus surface was deformed to about 10 nm, and the deformation increased continuously to 2 times after 48 h, and 10 times after 264-h treatments

at 50 °C (Fig. 5c, e). The torus deformed up to hundreds of nanometers after 648-h treatments: We conclude that the torus was fully degraded at this stage. The deformation was below 60 nm after 1344 h treatments at 20 °C, indicating a slower degradation rate. The deformation of the pit border surfaces showed only slight changes after 264-h of treatments at 50 °C, and remained below 60 nm after 648 h at 50 °C and 1344 h at 20 °C (Fig. 5d).

3.3 The acceleration effect of temperature

To show the relative change of the surface modulus with treatment time, we define the normalized residual modulus ratio E_r as:

$$E_r = \frac{E_t}{E_{t0\_ave}} \tag{3}$$

with E_{t0_ave} the average modulus of untreated samples, and E_t the modulus of samples treated at 50 °C for time t. An exponential curve was fitted to the modulus-treatment time relation at 50 °C (Fig. 5f):

$$E_r = 0.075 + 0.96 * \exp\left(-\frac{t + 2.9}{26.83}\right) \tag{4}$$

The R-squared is 0.97 and the reduced Chi-Square is 0.01.

From the fitted curve, the 107-h treatment at 50 °C corresponds to 1344-h treatment at 20 °C. Therefore, the degradation rate of the torus at 50 °C is about 10 times the rate at 20 °C.

3.4 Adhesion force

The torus is almost completely degraded after 648 h (see modulus and deformation in Fig. 5), so here the treatment time is considered up to 264 h in the following evaluations. The adhesion force and the jump-off force ratio show a linear relationship at each treatment time (except for the treatment time of 648 h). Here we define the linear spreading of the data points as the linear band; the untreated band (black points, Fig. 6) rotates clockwise with treatment time at 50 °C (Fig. 6a). The averages of adhesion forces show only small variations between treatment times (131–143 nN, Table 1). Therefore, the rotation of the bands is mainly caused by the increase of the jump-off force ratios.

To describe the rotation of the bands, each band was linearly fitted and the slopes of the fitted lines (band slope) at each treatment time are shown in Table 1. To show the relative change of the band slope with treatment time, we define the normalized residual band slope ratio,K_r as:

$$K_r = \frac{K_t}{K_{t0}} \tag{5}$$

with K_{t0} the band slope of untreated samples (black points in Fig. 6a), and K_t the band slope of samples treated at 50 °C for time t.

As shown in Fig. 6b, a linear relationship (Pearson's r = 0.93) was found between the residual band slope ratios and residual moduli ratios. The equation below shows that the modulus and the band slope (the adhesion force-jump off force ratio band) change approximately with the same rate:

$$E_r = 1.05(\pm 0.21) * K_r + 0.01(\pm 0.02) \tag{6}$$

The errors of the curve slope and intercept are shown in the parentheses. Pit torus is composed of mainly cellulose with a simple structure and a thickness of 100–300 nm [12, 28–30]. Therefore, the degradation of the torus can be considered as a reaction between a uniform cellulose membrane and the alkaline solutions, which results in a progressive and unidirectional change: the progressive decrease of the modulus (Fig. 5a); the progressive increase of the deformation (Fig. 5c, d) and the jump-off force ratio (Fig. 6a); the clockwise rotation of the band slope (adhesion force-jump off force ratio data points, Fig. 1a). [ab] The 1st and 2nd sigmoidal curves in the previous paper [27].

As shown in Fig. 6c, the adhesion forces and jump-off force ratios of a typical pit border show three distinct stages when treated in saturated calcium hydroxide solutions at 50 °C: the untreated stage I (black points); the stage 2 from the treatments for 1 to 264 h (between the red dashed curves); the stage 3 from the treatment for 648 h (blue points at the bottom). The pit border is formed by the over-arching secondary cell wall with cellulose aggregates embedded in the hemicelluloses-lignin matrix and small amounts of nonstructural components, such as extractives. Therefore, the surface properties are influenced by all the chemical components simultaneously, thus showing a different degradation process as the pit torus (Fig. 6a). In the previous paper [27], we found

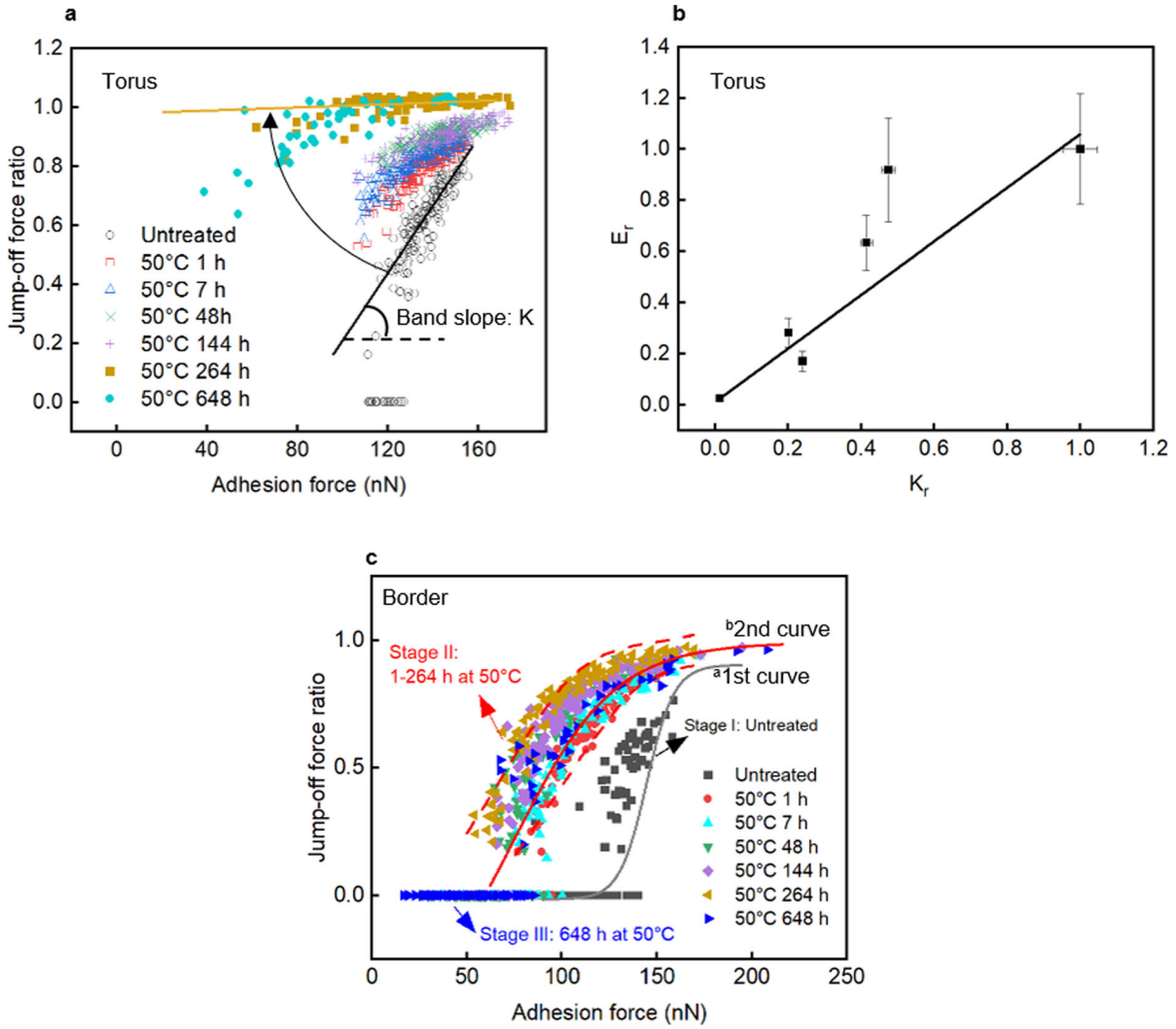

Fig. 6 The change in the adhesion force – jump-off force ratio of the pit torus and border with treatment time. **a** The pit torus. The black and yellow lines are to illustrate the slope of the bands; **b** The fitted line to the normalized modulus and the normalized slope; the squares represent averages and the vertical bars represent standard deviations; **c** The pit border. Stage I is from the untreated border. Stage II is from the border with the treatment time of 1, 7, 48, 144, and 264 h. During this treatment time, the modulus is degraded to 0.83–0.95 (the 95% CI) of untreated samples; Stage III is from the border with the treatment time of 648 h and the modulus is degraded to 0.20–0.23 (95% CI) of untreated samples. [ab] The 1st and 2nd sigmoidal curves in the previous paper [27]

two sigmoidal curves (the 1st and 2nd curves in Fig. 1c) to describe the shifting of data points (adhesion force, jump-off force ratio) after thermal treatments. The bottom part of the 1st curve represented an extractive-rich surface, and the adhesion forces ranged from 90 to150 nN. The bottom of the 2nd curve represented the exposure of cellulose aggregates after the degradation of the hemicelluloses-lignin matrix, and the adhesion forces ranged from 0 to 90 nN. The surface modulus (Fig. 5e) does not show a significant change after 1-h treatments, and changes to 0.83–0.95 (the 95% CI, Fieller's theorem [25]) of the untreated samples after the 264-h treatments ($P = 0.0009$). Therefore, the shift from the untreated stage I to the stage II (1–264 h, Fig. 6c) is not caused by the main structural components. It has been reported that wood extractives are released and might retard the cement hydration process [31–33].

Table 1 Adhesion forces and jump-off force ratios of the pit torus, and the slope K of the adhesion force-jump off force ratio bands with treatment time in Fig. 6a

Treatment time		Untreated	1 h	7 h	48 h	144 h	264 h
Average (Std[a])	F_{ad} (nN)[b]	135 (10)	137(11)	134(12)	143(12)	144(15)	131(23)
	I_{Fj}[c]	0.55 (0.23)	0.80 (0.07)	0.82 (0.07)	0.91 (0.04)	0.90 (0.05)	1.02 (0.01)
K_t (error)[d]	2.09 (0.10)	0.99 (0.04)	0.87 (0.03)	0.42 (0.02)	0.50 (0.02)	0.00 (0.00)	
K_r(error)	1.00 (0.047)	0.47 (0.018)	0.41 (0.016)	0.20 (0.010)	0.24 (0.011)	0.01 (0.007)	
Data size	171	171	171	171	171	92	

a: standard deviation, b: adhesion force, c: jump-off force ratio (see Fig. 3), d: the slope of the fitted line in the adhesion force-jump off force ratio band

We assume that the alkaline solutions remove the extractives from the pit border surface: This causes the data points to shift from the stage I to the stage II. The morphologies (Fig. 4) show that the border surface changes from the amorphous pattern to structures with particles. Correspondingly, the surface modulus decreased to 0.20–0.23 of the untreated samples (the 95% CI, Fieller's theorem [25]) after 648-h treatments. We assume that the shift from the stage II (264-h treatments) to the stage III (648-h treatments) indicates that the hemicelluloses-lignin matrix is degraded and the underlying cellulose aggregates are uncovered [27]. The cellulose aggregates turn into a loose structure without the cohesive matrix. The pit border is an over-arched secondary cell wall, and the cellulose aggregates are not aligned the same as in the unarched part [27] where regular parallel lines were shown. Therefore, we believe that the particles on the surface are clusters of cellulose aggregates after the removal of the extractives and the hemicelluloses-lignin matrix.Therefore, we conclude that the shifts in the adhesion forces and jump-off force ratios represent the degradation process of the border surface chemical components: the removal of the non-structural component extractives, the degradation of the hemicelluloses-lignin matrix and the exposure of the cellulose fibrils. This conclusion is inferred from the changes in surface morphologies and surface moduli of the pit border.

4 Discussion

The pit torus and border showed different degradation processes in the surface modulus, deformation, adhesion force and jump-off force ratio with treatment time in alkaline solutions. This indicates that AFM can be used to identify different structures and their degradation processes on the wood surface, namely pit border and pit torus. Adhesion forces can measure the surface chemical components: for the one-component pit torus, the adhesion forces of the cellulose membranes in the pit torus showed only small variations (131–143 nN, Table 1) after each treatment time – the pit torus has only one chemical component. The adhesion forces measured on the pit border (the over-arching secondary cell wall) showed three stages of degradation. We conclude that these three stages indicate the degradation of extractives, the hemicelluloses-lignin matrix, and the exposure of the cellulose aggregates — the different chemical components dominate the adhesion forces when they are exposed on the surface during the degradation process (when the extractives are degraded, the hemicelluloses-lignin matrix is exposed; when the matrix is degraded, the cellulose fibrils are exposed. Fig 6c).The surface modulus, deformation, the jump-off force ratio, and the band slope (adhesion force and jump-off force ratio data points) are sensitive to the degradation of the main structural components, such as the hemicelluloses-lignin matrix in the pit border and the cellulose in the pit torus. The non-structural components extractives have no influence on the surface modulus of the pit border.A good match was found between the topography, surface modulus, deformation, the jump-off force ratio, and the band slope (adhesion force-jump off force ratio data points) during the degradation process of the torus. When the pustules on the torus surface were dissolved, and the cohesive matrix between cellulose aggregates on the border surface

was removed (Fig. 4), the surface modulus, deformation, the jump-off force ratio, and the band slope changed correspondingly. Especially, the surface modulus and the band slope in the torus changed almost synchronously with treatment time (Fig. 6-b).When the cement hydrates, ions such as OH^- and Ca^{2+} are released into the water phase. The hydration process releases heat and causes the temperature to rise to 50 °C or higher. In the timber-concrete composite, the wood surface is in direct contact with the alkaline environment with the elevated temperature, after the concrete is poured and starts to cure. The 7-h treatments already degraded the pit torus significantly (0.61–0.66 of the untreated samples, the 95% CI), and 48-h treatments could be deemed to degrade the torus almost completely (Fig. 5a). Therefore, the torus is easily degraded during the cement hydration process. This can facilitate the dissolved alkaline ions to transport further into the material in time.The alkaline environment with elevated temperature in cement for 10 days degrades the pit border slightly: the border surface modulus changes to 0.83–0.95 (the 95% CI) of untreated samples; But 27-day treatments will cause an almost complete loss in the modulus (Fig. 5b). The pit border is formed by the secondary cell wall, and is not damaged by the cutting with a diamond knife, so the border surface represents the secondary cell wall in the natural state. The degradation of the pit torus at 50 °C is about 10 times faster than at 20 °C. Due to the complex structure and the chemical components we were not able to establish the acceleration effect of temperatures for the pit border.

5 Conclusion

AFM can measure the degradation process of different wood structures and wood components during alkaline treatments. The adhesion force could indicate the change of the surface material during degradation. The surface modulus, deformation, the jump-off force ratio, and the band slope (adhesion force and jump-off force ratio data points) could indicate the degradation of structural components of the surface. These parameters showed a good match during the degradation process. In the fresh poured timber-concrete composites, several hours of increased temperature and the alkaline environment could degrade the torus membrane almost completely. The degraded pit torus can cause an easier transport of alkaline ions into the inner part of the wood. The temperature of 50 °C caused about 10-times faster degradation of the torus compared to 20 °C in the alkaline solutions. The surface modulus of the pit border degraded to 0.83–0.95 (the 95% CI) of untreated samples after 10 days and to 0.20–0.23 of the untreated samples after 27 days of treatments.

Acknowledgements This research was partially funded by the German Research Foundation (DFG) as a part of the Graduiertenkolleg 2075. The Fraunhofer Wilhelm-Klauditz-Institute provided access to the AFM and FTIR equipment. The authors express thanks to Peter Hardi and his help with the SEM. The help of Martina Zühlke with the nitrogen gas is gratefully acknowledged.

Author contributions J.L. designed the experiments, prepared the materials and performed the experiments. J.L. analyzed the data and wrote the manuscript. B.K. directed the research and revised the manuscript.

Funding Open Access funding enabled and organized by Projekt DEAL.

Declarations

Competing interests The authors declare no competing financial interest.

References

1. Yeoh D, Fragiacomo M, de Franceschi M et al (2011) State of the art on timber-concrete composite structures: Literature review. J Struct Eng 137(10):1085–1095. https://doi.org/10.1061/(ASCE)ST.1943-541X.0000353
2. Stapper JL, Gauvin F, Brouwers H (2021) Influence of short-term degradation on coir in natural fibre-cement composites. Constr Build Mater 306:124906. https://doi.org/10.1016/j.conbuildmat.2021.124906

3. Gram H-E (1983) Durability of natural fibres in concrete. Swed Cem Concr Res Inst, Stockh 1(83):255
4. Onuaguluchi O, Banthia N (2016) Plant-based natural fibre reinforced cement composites: A review. Cem Concr Compos 68:96–108. https://doi.org/10.1016/j.cemconcomp.2016.02.014
5. Govin A, Peschard A, Fredon E et al (2005) New insights into wood and cement interaction. Holzforschung 59(3):330–335. https://doi.org/10.1515/HF.2005.054
6. Oka D, Kobayashi K, Isobe N et al (2013) Enzymatic hydrolysis of wood with alkaline treatment. J Wood Sci 59(6):484–488. https://doi.org/10.1007/s10086-013-1359-x
7. Wei J, Meyer C (2015) Degradation mechanisms of natural fiber in the matrix of cement composites. Cem Concr Res 73:1–16. https://doi.org/10.1016/j.cemconres.2015.02.019
8. Melo Filho JdA, Silva FdA, Toledo Filho RD (2013) Degradation kinetics and aging mechanisms on sisal fiber cement composite systems. Cem Concr Compos 40:30–39. https://doi.org/10.1016/j.cemconcomp.2013.04.003
9. Mardmomen S (2020) On-site measurement of the water-cementitious ratio and heat of hydration of delivered concrete. Dissertation, West Virginia University
10. Do T.A. (2013) Finite element modeling of behavior of mass concrete placed on soil. Dissertation, University of Florida.
11. Burr HK, Stamm AJ (1947) Diffusion in wood. J Phys Colloid Chem 51(1):240–261
12. Choat B, Cobb AR, Jansen S (2008) Structure and function of bordered pits: new discoveries and impacts on whole-plant hydraulic function. New Phytol 177(3):608–626. https://doi.org/10.1111/j.1469-8137.2007.02317.x
13. Bauch J, Liese W, Schultze R (1972) The morphological variability of the bordered pit membranes in gymnosperms. Wood Sci Technol 6(3):165–184. https://doi.org/10.1007/BF00351575
14. Dute RR, Elder T (2011) Atomic force microscopy of torus-bearing pit membranes. IAWA J 32(4):415–430. https://doi.org/10.1163/22941932-90000068
15. Lehringer C, Hillebrand K, Richter K et al (2010) Anatomy of bioincised Norway spruce wood. Int Biodeterior Biodegrad 64(5):346–355. https://doi.org/10.1016/j.ibiod.2010.03.005
16. Pesacreta TC, Groom LH, Rials TG (2005) Atomic Force Microscopy of the Intervessel Pit Membrane in the Stem of Sapium Sebiferum (Euphorbiaceae). IAWA J 26(4):397–426. https://doi.org/10.1163/22941932-90000124
17. Lee J, Holbrook NM, Zwieniecki MA (2012) Ion induced changes in the structure of bordered pit membranes. Front Plant Sci 3:55. https://doi.org/10.3389/fpls.2012.00055
18. Mao J, Abushammala H, Kasal B (2021) Monitoring the surface aging of wood through its pits using atomic force microscopy with functionalized tips. Colloids Surf, A 609:125871. https://doi.org/10.1016/j.colsurfa.2020.125871
19. Cappella B, Dietler G (1999) Force-distance curves by atomic force microscopy. Surf Sci Rep 34(1–3):1–104. https://doi.org/10.1016/S0167-5729(99)00003-5
20. Hertz H (1881) Ueber die berührung fester elastischer körper. J für die reine und angew Math (Crelles J) 92:156-171. https://doi.org/10.1515/crll.1882.92.156
21. Kopycinska-Müller M, Geiss RH, Hurley DC (2006) Contact mechanics and tip shape in AFM-based nanomechanical measurements. Ultramicroscopy 106(6):466–474. https://doi.org/10.1016/j.ultramic.2005.12.006
22. Li J, Kasal B (2021) Repeatability of adhesion force measurement on wood longitudinal cut cell wall using atomic force microscopy. WFS 53(1):3–16. https://doi.org/10.22382/wfs-2021-02
23. OriginLab Corporation Origin(Pro), Northampton, MA, USA
24. IBM Corp. IBM SPSS Statistics for Windows, Armonk, N.Y USA
25. Fieller EC (1954) Some problems in interval estimation. J Roy Stat Soc: Ser B (Methodol) 16(2):175–185. https://doi.org/10.1111/j.2517-6161.1954.tb00159.x
26. Nečas D, Klapetek P (2012) Gwyddion: an open-source software for SPM data analysis. Open Phys. https://doi.org/10.2478/s11534-011-0096-2
27. Li J, Kasal B (2022) Effects of thermal aging on the adhesion forces of biopolymers of wood cell walls. Biomacromolecules 4:1601–1609. https://doi.org/10.1021/acs.biomac.1c01397
28. Boyce CK, Zwieniecki MA, Cody GD et al (2004) Evolution of xylem lignification and hydrogel transport regulation. Proc Natl Acad Sci USA 101(50):17555–17558. https://doi.org/10.1073/pnas.0408024101
29. Jansen S, Choat B, Pletsers A (2009) Morphological variation of intervessel pit membranes and implications to xylem function in angiosperms. Am J Bot 96(2):409–419. https://doi.org/10.3732/ajb.0800248
30. Plavcová L, Jansen S, Klepsch M et al (2013) Nobody's perfect: can irregularities in pit structure influence vulnerability to cavitation? Front Plant Sci 4:453. https://doi.org/10.3389/fpls.2013.00453
31. Pehanich JL, Blankenhorn PR, Silsbee MR (2004) Wood fiber surface treatment level effects on selected mechanical properties of wood fiber–cement composites. Cem Concr Res 34(1):59–65. https://doi.org/10.1016/S0008-8846(03)00193-5
32. Castro VG, Da Azambuja RR, Bila NF et al (2018) Correlation between chemical composition of tropical hardwoods and wood-cement compatibility. J Wood Chem Technol 38(1):28–34. https://doi.org/10.1080/02773813.2017.1355390
33. Vaickelionis G, Vaickelioniene R (2006) Cement hydration in the presence of wood extractives and pozzolan mineral additives. Ceram - Silik 50(2):115–122